ELSEVIER

Contents lists available at ScienceDirect

Composites: Part A

journal homepage: www.elsevier.com/locate/compositesa



Process-induced fiber matrix separation in long fiber-reinforced thermoplastics



S. Goris*, T.A. Osswald

Polymer Engineering Center, Mechanical Engineering Department, University of Wisconsin-Madison, USA

ARTICLE INFO

Article history:
Received 17 September 2017
Received in revised form 21 November 2017
Accepted 25 November 2017
Available online 5 December 2017

Keywords:
A. Glass fibres
B. Microstructures
D. Microstructural analysis
E. Injection molding

ABSTRACT

This work explores the fiber migration during injection molding of long glass fiber-reinforced polypropylene. It was found that the simplified assumption of uniform fiber concentration distribution is inaccurate, and the process causes substantial variations in the fiber concentration along the flow path and through the thickness of injection molded parts. This was tested for a simple plate geometry molded at varying nominal fiber concentrations. The fiber concentration was measured by pyrolysis to obtain a global concentration, and using micro computed-tomography for a through-thickness analysis. Additionally, the fiber concentration at the melt front of partially filled moldings was investigated. A new measurement protocol using micro computed-tomography and digital image processing is proposed to calculate the through-thickness fiber concentration. The results of this study show substantial heterogeneity of the fiber concentration throughout the molded plates. Fibers agglomerated in the core layer with volume fractions up to 1.5 times the nominal fiber concentration.

© 2017 Elsevier Ltd. All rights reserved.

1. Introduction

Injection molding using long fiber-reinforced thermoplastics (LFTs) is a widely-used process to manufacture parts with enhanced mechanical properties. Particularly in the automotive industry, LFTs have gained importance due to their exceptional lightweight properties and cost-efficient manufacturing processes. With favorable specific stiffness and strength, LFT materials can potentially replace metals for structural applications and play a key role in reducing the overall weight of automobiles. However, the local properties and global performance of the molded part greatly depend on the final state of the fibers [1,2]. During mold filling, the configuration of the fibers changes significantly, reflected in mechanisms referred to as fiber attrition, fiber orientation, fiber jamming and fiber matrix separation [3–5]. In particular, the phenomenon of fiber matrix separation, which describes the process-induced variation of fiber concentration, has not been fully understood. Fiber migration during processing occurs on two scales - variation in fiber local concentration through the thickness of a molded part and global concentration gradient along the flow path.

Previous studies have addressed the process-induced concentration gradients throughout molded parts for filled thermoplas-

E-mail addresses: sgoris@wisc.edu (S. Goris), tosswald@wisc.edu (T.A. Osswald).

tics, including short fiber (aspect ratio <100) and long fiber (aspect ratio >100) reinforced composites. Toll and Andersson [6] published results showing an increase in fiber concentration from nominal 30 wt.% in the raw material to 36 wt.% at the end of the flow path of a film-gated plate for glass fiber-reinforced polyamide 66 (PA66). In a similar study, O'Regan et al. [7] observed an increase of 3-4 vol.% at the end of the flow path in injection molding of fiber-reinforced PA66. Lafrance et al. [8] showed an increase from 39 wt.% at the gate to 51 wt.% at the end of the flow path for a fan-gated plate. Using a spiral mold, Kubat and Szalanczio [9] studied the filler migration effects of a glass sphere-filled low-density polyethylene. Along a total length of up to 1950 mm, they measured the filler concentration and found substantial migration of the particles towards the end of the flow path. Their results suggest a relative increase of up to 25% filler concentration at the tip of the spiral for glass spheres with diameters between 53 and 105 µm.

Hegler and Menning [10] published work on the filler separation effects during injection molding of glass bead and glass fiber-filled thermoplastics using dumbbell and rectangular box specimens. Their results show that the separation effects were more pronounced with beads than with fibers indicating an influence of the shape and dimensions of the fillers. Furthermore, they conclude that mold geometry and filler concentration are key parameters determining the degree of filler migration in injection molding. Other processing parameters, such as mold temperature, injection speed, matrix material and screw speed did not

^{*} Corresponding author.

substantially impact the filler-matrix separation phenomena in their experiments.

Ogadhoh and Papathanasiou [11] studied particle migration during mold filling of glass bead-filled polystyrene with an average bead size varying from 50 to 500 µm. Their results agree with previous studies, showing the filler matrix separation increases substantially with larger beads with the largest relative increase of 15% more fillers for 500 µm glass beads at the end of the flow. Another major outcome of their work was the observation that particles appear to accumulate at the free surface. For the largest particle sizes used in the study, the concentration of particles near the free surface was almost double than in the feed material. Their results on filler migration strongly indicate a dependency of particle size and nominal concentration.

Mondy et al. [12] conducted fiber migration experiments in a wide-gap Couette flow for low aspect ratio nylon fibers in glycol. Their measurements show a migration of fibers to the low-shear regions. While the authors did not find an impact of aspect ratio on the migration, they found an influence of fiber concentration suggesting that the effect of shear-migration increases at elevated concentrations.

The common conclusion of all studies is the outcome that the fiber concentration increases towards the end of the flow path, suggesting that the last filled location carries an accumulated amount of filler. Furthermore, the processing conditions appear to play a smaller role for the degree of fiber matrix separation. The influencing factors are reported to be both the concentration and the shape of the filler since the migration effect is more pronounced for longer fibers than it is for shorter fibers [6].

The through-thickness filler concentration gradient in injection molding has been addressed much less frequently. A first comprehensive study was conducted by Toll and Andersson [6] for 30 wt.% glass fiber-reinforced PA66 and simple plate geometry. They found an agglomeration of fibers in the core layer using a sectioning and microscopic measurement protocol. Their results suggest almost 40% more fibers in the core layer than in the shell for their long fiber PA66 (initial fiber length of 10 mm). For the short fiber grade (initial fiber length of 0.6 mm), the fiber agglomeration is much less pronounced with only 10% more fibers in core than in the shell region

While other publications also mention the phenomenon of fiber agglomerating in the core of injection molded part, the observations are mostly side-effects in these studies; no comprehensive analysis exists nor have theories been formulated to explain the underlying mechanism. Velez-Garcia et al. [13] focused on fiber orientation measurements for short fiber-reinforced polybutylene terephthalate (PBT) by applying a newly developed sectioning procedure. From the obtained micrographs, they also reported a fiber concentration gradient through the thickness of the molded center-gated disk. Recently, Sun et al. [14] published an experimental study on using micro computed-tomography (µCT) to quantify the fiber orientation of an LFT injection molded instrument panel. While also focusing on orientation measurements, they incidentally analyzed the pixel fraction from µCT scans indicating a strong agglomeration of fibers in the core layer of the molded part.

Theoretical models to describe particle migration in concentrated suspensions have been proposed. Leighton and Acrivos [15] suggested a diffusive flux model, which describes the shear-induced particle migration as a result of irreversible particle collisions. This kinematic modeling approach expresses the migration as gradients of particle concentration and shear rate, but it neglects normal stress differences.

Nott and Brady [16] proposed a suspension balance model. This model is a two-phase approach describing the particle phase and suspension separately while incorporating a constitutive model

to solve particle and suspension stresses. The particle transport is driven by gradients in these stresses. Morris and Boulay [17] expanded the suspension balance model to account for anisotropic migration. The latter model was recently implemented in a commercially injection molding simulation software (Moldex3D™, CoreTech Systems, Taiwan). Using this three-dimensional (3D) finite volume method (FVM) solver, Tseng et al. [18,19] simulated the fiber migration for a short fiber-reinforced PBT. Their results suggest that the model can qualitatively predict the tendency of the process-induced fiber concentration in the molded part. However, there are still quantitative discrepancies in the through-thickness prediction of the fiber concentration. Also, their work does not address the relevance of the suspension models fitting parameters nor how to obtain appropriate values for these parameters for fiber-reinforced thermoplastics.

Fiber matrix separation can also be caused by the part design and the features of the part. The separation effect in rib-filling has been studied by a few research groups, who describe the phenomenon of fibers accumulating in the base of the rib while the tip of the rib remains almost fiber-free [5]. While this is an important field of research, the impact of design features on fiber matrix separation is not part of this work and the reader is referred to a recent publication on rib-filling [20].

A major challenge has been, and remains to be, the availability of reliable measurement techniques that allow a comprehensive analysis of fiber concentration for sufficiently large samples in a timely manner. The full characterization of the 3D fiber microstructure for fiber-reinforced composites has not been standardized yet and differences in characterization protocols question the comparability of experimental studies. However, reliable experimental data is necessary to understand the underlying physics of fiber matrix separation, to develop new models to predict the process-induced fiber matrix separation in LFT injection molding and to validate predictive tools.

This work presents a comprehensive experimental study on the fiber matrix separation in LFT injection molding for a simple plate geometry at varying nominal fiber concentration. A measurement protocol using μ CT and image processing is introduced for the characterization of the through-thickness fiber concentration. The analysis of the fiber concentration at the flow front was performed to obtain experimental data of the reorientation of the fibers in the fountain flow region and the corresponding impact on the final fiber concentration distribution.

2. Materials and methods

The material used in this study is a commercially available long glass fiber-reinforced polypropylene (PPGF) (SABIC[®] STAMAX[™]). Table 1 summarizes the main material properties.

The design-of-experiments (DoE) consists of nominal fiber concentrations varying from 5 wt.% to 60 wt.% Table 2 summarizes the trial label, the corresponding fiber volume and fiber weight concentration as well as the raw material used to achieve the respective nominal concentrations. PPGF20, PPGF30, PPGF40 and PPGF60 are provided as compounded pellets by the material supplier (coated long fiber pellets). PPGF05, PPGF10 and PPGF50 were achieved by mixing higher fiber concentrations with neat PP

Table 1SABIC® STAMAX™ LFT material properties according to the material supplier [21].

Material property	Value
Nominal fiber length [mm] Fiber diameter [µm]	15.0 19 + 1
Density of fibers [g/cm ³] Density of PP [g/cm ³]	2.55 0.905

 Table 2

 Summary injection molding trials: Nominal fiber concentration and raw material.

Trial label	Weight concentration	Volume concentration	Feed material
PPGF05	5 wt.%	1.8 vol.%	25% PPGF20 and 75% neat PP
PPGF10	10 wt.%	3.8 vol.%	50% PPGF20 and 50% neat PP
PPGF20	20 wt.%	8.2 vol.%	STAMAX [™] 20YM240
PPGF30	30 wt.%	13.2 vol.%	STAMAX™ 30YM240
PPGF40	40 wt.%	19.1 vol.%	STAMAX [™] 40YM240
PPGF50	50 wt.%	26.2 vol.%	83% PPGF20 and 17% neat PP
PPGF60	60 wt.%	34.7 vol.%	STAMAX™ 60YM240

 Table 3

 Processing conditions for the injection molding trials.

Molding parameter	Value
Melt temperature [°C]	250
Mold temperature [°C]	50
Back pressure [bar]	5
Injection time [s]	2
Holding pressure [bar]	300
Holding time [s]	22

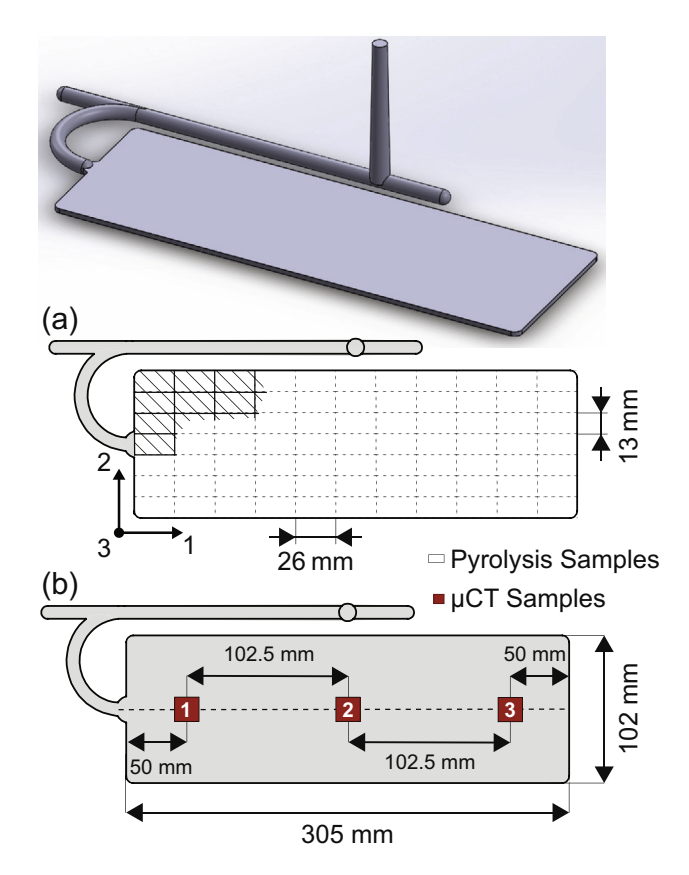


Fig. 1. Sketch of the plate geometry and illustration of the sample locations for the microstructure analysis. The sample locations for the through-thickness fiber concentration analysis are along the center line of the plate: location 1 (close to the gate), location 2 (center of the plate), and location 3 (end of the flow). (For interpretation of the references to color in this figure legend, the reader is referred to the web version of this article.)

(SABIC[®] PP 579S) in a cement mixer before feeding it into the hopper of the injection molding machine. The neat PP is the same as the matrix material of the coated long fiber STAMAX™ pellets.

The parts were molded on a 130-ton Supermac Machinery SM-130 injection molding machine. The processing settings followed the suggest processing guidelines by SABIC® [22] and are summarized in Table 3.

The part geometry used in this study is a simple plate with dimensions of $102 \times 305 \times 2.85 \text{ mm}^3$. The cavity is filled through a 20 mm edge-gate, which is fed through a 17 mm round runner as illustrated in Fig. 1.

The fiber concentration analysis focuses on two measurement protocols. First, the global concentration variation throughout the entire part was measured through pyrolysis by extracting 13 \times 26 \times 2.85 mm^3 samples as illustrated in Fig. 1(a). Second, the through-thickness fiber concentration was obtained using μCT for three samples along the center line with dimensions of 10 \times 15 \times 2.85 mm^3 , as shown in Fig. 1(b).

Additional trials at a nominal fiber concentration of 40 wt.% (PPGF40) with partial mold fillings (short shots) were conducted at the same processing conditions without a packing phase to study the fiber concentration at the flow front. Fig. 2 shows photographs of partially molded parts and the relative sample locations, which are 3 mm, 10 mm and 17 mm from the advancing flow front. Additional measurements of the local fiber concentration through pyrolysis were performed to obtain the fiber concentration gradient along the flow length. Slices between 5 mm and 15 mm were cut from a 20 mm wide strip along the center line of the partial mold fillings (Fig. 2).

3. Measurement protocols

The most common approach to determine the local fiber concentration is thermal degradation of the matrix material and measuring the remaining weight of the fibers to calculate the weight fraction. However, a fairly new approach is to use μ CT data to analyze the fiber concentration through the part thickness using image processing. Both procedures are applied in this study to obtain a full characterization of the fiber concentration gradient throughout the molded parts.

3.1. Global concentration gradient analysis using pyrolysis

The global fiber concentration throughout the molded part was determined by extracting samples and matrix removal in a muffle furnace at $600\,^{\circ}\text{C}$ for 1.5 h. The weight fraction of the remaining fiber was determined on a high precision scale and converted in volume fraction by

$$\phi_{volf} = \frac{\frac{\phi_{wtf}}{\rho_f}}{\frac{\phi_{wt,m}}{\rho_f} + \frac{\phi_{wt,m}}{\rho_m}} \tag{1}$$

where $\phi_{wt,f}$ and $\phi_{wt,m}$ are the weight fractions of the fibers and the matrix, respectively, and ρ denotes the density of fibers (f) and matrix (m). The measurements were repeated five times for each trial

3.2. Through-thickness concentration analysis using μ CT

 μ CT is a non-destructive testing method based on X-ray imaging to inspect the internal structure of a sample and to evaluate its properties. The advantage of μ CT is that it can achieve a full 3D representation on a small scale without destroying the specimen. The basic principle of μ CT is to irradiate a sample with penetrating X-rays, which are attenuated and captured downstream of the object with a detector system creating radiographs. The specimen, which is fixed on a rotating platform, is irradiated at various angles to achieve a full representation of the specimen. The

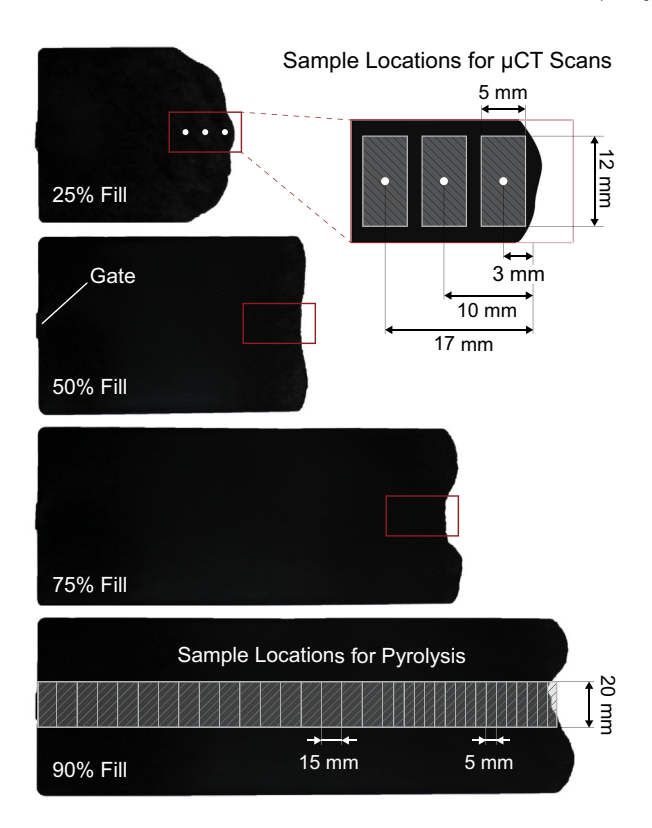


Fig. 2. Flow front analysis: PPGF40 short shots (photos) and sample location at the flow front. (For interpretation of the references to color in this figure legend, the reader is referred to the web version of this article.)

detector records the attenuated X-rays and their intensity distribution is directly related to the material's atomic density. Subsequently, a 3D reconstruction of the sample is generated from all radiographs using tomographic reconstruction. The 3D reconstruction or μ CT data set can then be further processed for qualitative and quantitative analysis of the specimen. For more detailed information, the reader is directed to Stock [23].

The samples were scanned with an industrial µCT system (Metrotom 800, Carl Zeiss AG, Germany). The resolution (voxel size) of the scan is an important parameter that determines the accuracy of the measurements. However, the trade-off between scan resolution and sample size needs to be taken into account. In general, finer scan resolutions reduce the scan volume. Although a very fine resolution might be needed for an accurate analysis, a small sample might not fully represent the local fiber configuration, especially for long fiber-filled materials. In the literature, there is a wide variety of suggested scan resolutions and sample dimensions ranging from 3 µm voxel size resolution (sample size: 4 mm disk with a thickness of 4 mm) [24] up to a voxel size of 40 μm (sample size: $40 \times 40 \times 30 \text{ mm}^3$) [25]. The scan resolution for this work was set to 5.25 μm and the sample dimensions are 10 \times $15 \times 2.85 \text{ mm}^3$. Since the fiber diameter of the material is 19 μm , single fiber filaments can be clearly identified in the scans. A pretrial analysis was performed to investigate the impact of resolution on the results of the analysis by varying the resolution between 2 μm to 10 μm for identical samples. The analysis showed that the outcome of the analysis is not changed within this range. Table 4 summarizes the scan parameters used for all subsequent measurements.

The obtained μ CT data sets are processed to determine the change of fiber concentration through the sample thickness by applying an image processing algorithm. The process flow chart of the procedure is illustrated in Fig. 3. First, the raw μ CT data

Table 4 Zeiss Metrotom 800 scan parameters.

Parameter	Value	
Voltage [kV]	50	
Current [µA]	80	
Integration time [ms]	1000	
Gain [-]	8.0	
Spot size [µm]	5.0	
Voxel size [µm]	5.25	

set is aligned and registered using VG StudioMAX 3.0 (VolumeGraphics, Heidelberg, Germany). Subsequently, the data set is exported as an image stack (2D slices) oriented normal to the thickness direction. Each 2D slice represents a thickness equal to the resolution of the μ CT (5.25 μ m). The 2D slices comprising grayscale images are imported into MATLAB (MathWorks, Natick, USA) and the fiber volume fraction through the thickness of the sample is calculated by a developed algorithm described in the following paragraphs.

The grayscale images are transformed into binary images by segmentation, which requires selecting a reasonable threshold value to separate each image into black (matrix) and white (fibers) pixels as shown in Fig. 4 (left). In the grayscale 2D slice, each pixel with the coordinates (x,y) has a distinct grayscale value f(x,y), which depends on the bit depth (e.g. a 16-bit grayscale image has 65,536 tonal levels). A basic thresholding approach is to separate the grayscale image into a binary image by setting a global threshold value. The value for each pixel in the binary image is calculated by

$$g(x,y) = \begin{cases} 0, & \text{if } f(x,y) > T_k \\ 1, & \text{if } f(x,y) \leqslant T_k \end{cases}$$
 (2)

where T_k is the relative grayscale value for thresholding. For each 2D slice z, the fiber volume fraction $\phi_f(z)$ is calculated by the fraction of white pixels of the entire image $N \times M$:

$$\phi_f(z) = \frac{\sum_{i=1}^{n} \sum_{j=1}^{m} g(x_i, y_j)}{N \times M}$$
(3)

The true T_k is unknown due to the gradual change in the grayscale value between the two phases as illustrated in Fig. 4 (left). The choice of the threshold directly determines the size of the segmented phases and, thus, the fiber volume concentration. Even at very fine resolutions, the true threshold value cannot be detected directly from the μ CT data set. A heuristic procedure for the segmentation is proposed by calculating the threshold value as the midpoint between the mean value representing the fibers and the mean value of the background. This selection might not result in the true threshold value, but any uncertainty around the value would merely shift the obtained fiber volume concentration as shown in Fig. 4 (center). Hence, selecting a single value for T_k and performing a normalization step for the entire image stack (μ CT data set) resolves the ambiguity in selecting the true threshold value.

The average fiber concentration of the entire μ CT data set $\overline{\phi_f}$ is calculated from the individual fiber volume concentration $\phi_f(z)$ of each slice. The normalized fiber concentration distribution $\phi_f^n(z)$ can be obtained for each image as follows

$$\phi_f^n(z) = \frac{\phi_f(z)}{\overline{\phi_f}} \tag{4}$$

For a wide range of values for T_k , the normalized fiber concentration distribution is the same, as shown in Fig. 4 (right). Only at extreme values, where $T_k < 0.3$ or $T_k > 0.7$, skewed distributions are seen. With this approach, it is possible to accurately obtain

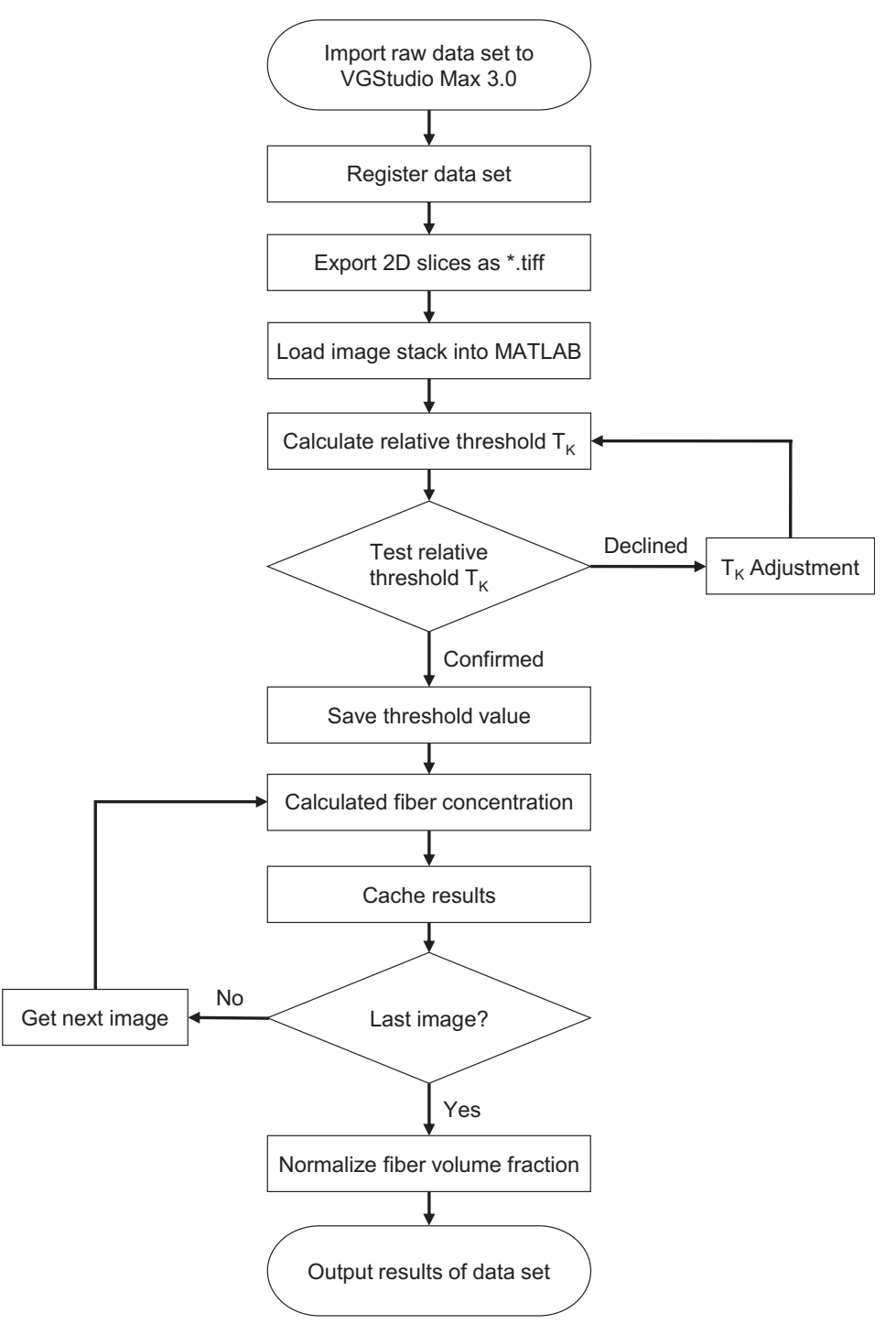


Fig. 3. Flow chart of the procedure for the through-thickness concentration analysis.

the through-thickness fiber concentration from μCT data. If needed, absolute values for the fiber concentration distribution can be calculated by measuring the local fiber concentration of the entire sample through pyrolysis.

3.3. Validation of the image processing analysis

The proposed measurement protocol for the through-thickness fiber concentration analysis using μCT was validated by performing a milling and pyrolysis procedure. After the μCT scan of a sample, the identical sample was milled down in defined increments of 0.2 mm along the thickness. The shavings

were carefully collected using a vacuum setup and a 25 μ m mesh to ensure capturing all material during milling. The fiber weight concentration for each layer was determined by measuring the sample weight before and after pyrolysis on a high precision scale Explorer® (Ohaus, Parsippany, USA) with an accuracy of ± 0.01 mg. After converting the obtained measurements to volume fraction, the results from the μ CT measurements and from the pyrolysis were compared. The validation was performed for samples at a nominal fiber weight fraction of 20 wt.% (PPGF20) and 40 wt.% (PPGF40) extracted at the center location of the molded plate. The procedure was repeated three times for each sample.

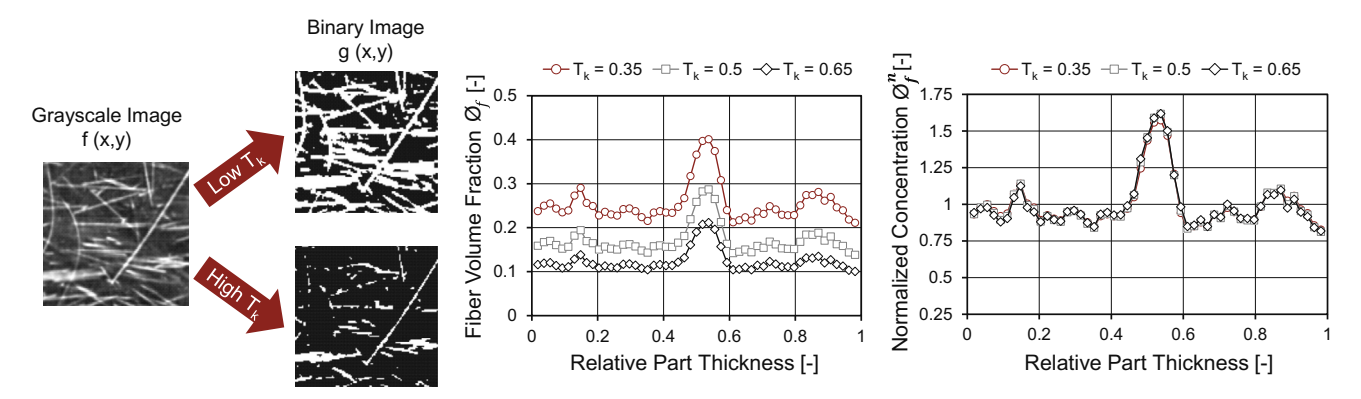


Fig. 4. Transforming a grayscale image into a binary image (left), the obtained fiber volume fraction for varying relative threshold values (center), and the normalized fiber concentration distribution (right). (For interpretation of the references to color in this figure legend, the reader is referred to the web version of this article.)

The outcome of the comparison is shown in Fig. 5. The results show strong agreement between the two measurement procedures. Discrepancies between the results from the milling procedure and the μ CT analysis are less than 2.5% for each of the six samples. Hence, the proposed μ CT analysis protocol is suitable to accurately and efficiently quantify the fiber concentration through the thickness of the part. The μ CT approach is non-destructive for the extracted sample and allows additional testing. Furthermore, it is also a faster analysis of the μ CT-thickness fiber concentration and allows for fiber orientation analysis of the same μ CT data set. However, the investment costs for μ CT is still large [26], making this approach more expensive than a conventional procedure using subtractive machining.

3.4. Fiber packing density analysis

The average distance between fibers was determined from the μ CT scans to obtain a better understanding of the fiber packing density. For each individual fiber in the 2D slices, the distance of the closest adjacent fiber is determined by performing the nearest neighborhood algorithm in the image processing software Fiji [27], as illustrated in Fig. 6. The analysis was done for the center location

of all samples. The shell and the core layer were analyzed separately for each sample by processing 2D slices of the in-flow direction and the cross-flow direction separately. Hence, the fibers in the corresponding layer are sliced perpendicularly, leading to a circular shape in the 2D slice, which improves the accuracy of the nearest neighborhood analysis.

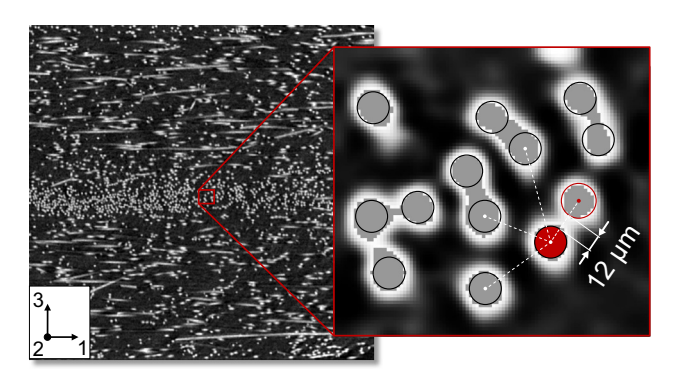


Fig. 6. Illustration of the packing density analysis using the nearest neighborhood algorithm. (For interpretation of the references to color in this figure legend, the reader is referred to the web version of this article.)

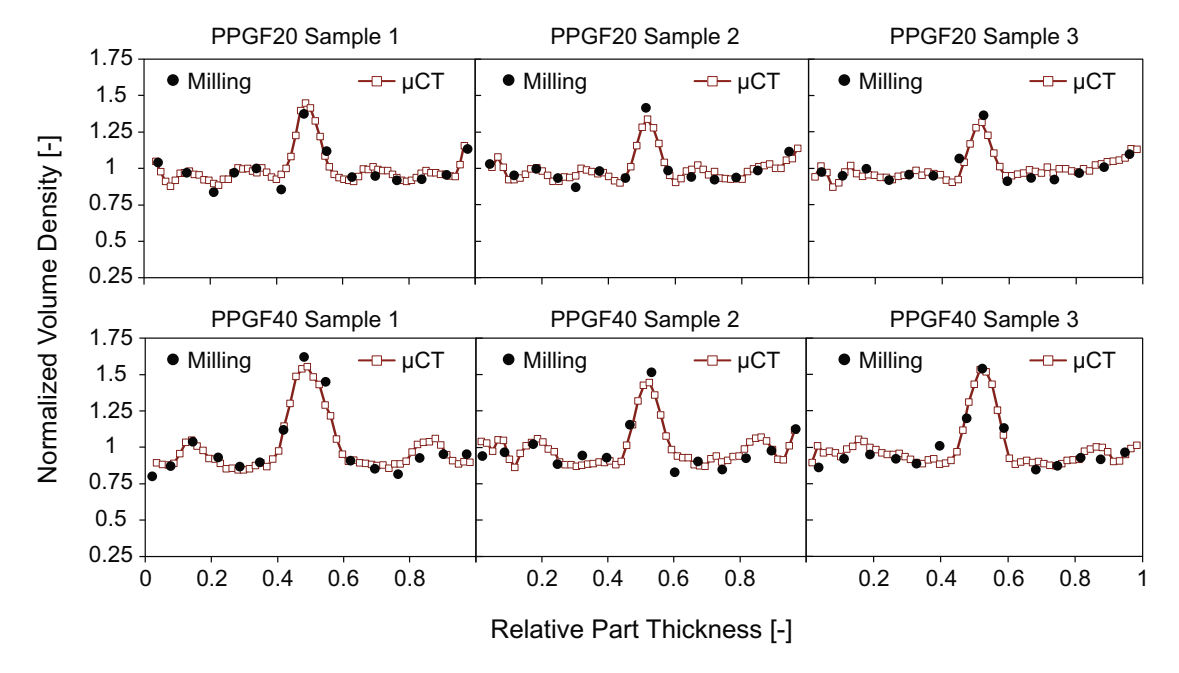


Fig. 5. Comparison of the milling procedure and μ CT analysis for the through-thickness fiber concentration measurements. (For interpretation of the references to color in this figure legend, the reader is referred to the web version of this article.)

4. Results

4.1. Global concentration gradient analysis using pyrolysis

The global fiber concentration variation throughout the molded plates was determined by pyrolysis. The measurements for each trial were repeated three times. The results are depicted as relative variation to the nominal fiber volume concentration. As expected, the uniform filling pattern and the simple part geometry result in symmetric global fiber concentrations as shown in the obtained results for PPGF30 in Fig. 7. The average value for each trial is calculated by averaging along the symmetry axis and averaging three repeated measurements as illustrated in Fig. 7, which shows a strong repeatability for all trials.

The results for all trials are shown in Fig. 8. The measurements show regions of low and elevated fiber concentration for each trial.

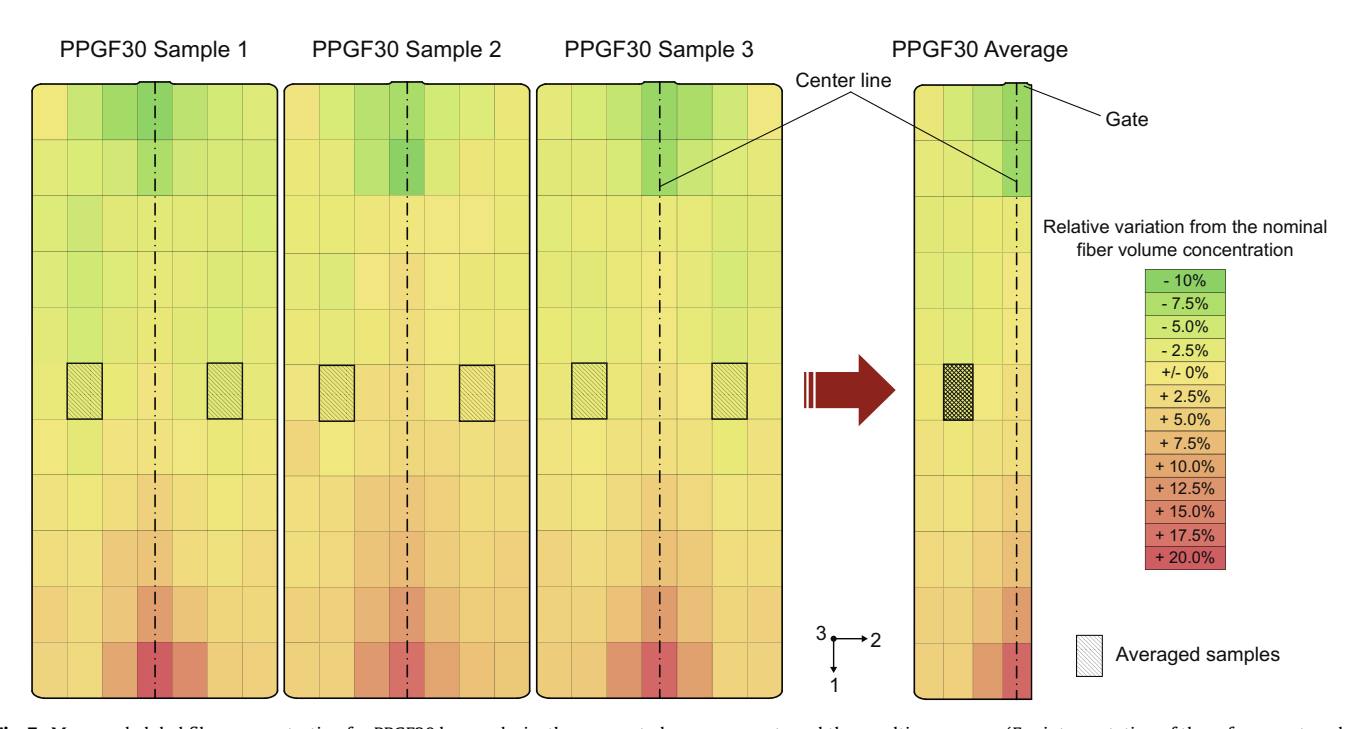


Fig. 7. Measured global fiber concentration for PPGF30 by pyrolysis: three repeated measurements and the resulting average. (For interpretation of the references to color in this figure legend, the reader is referred to the web version of this article.)

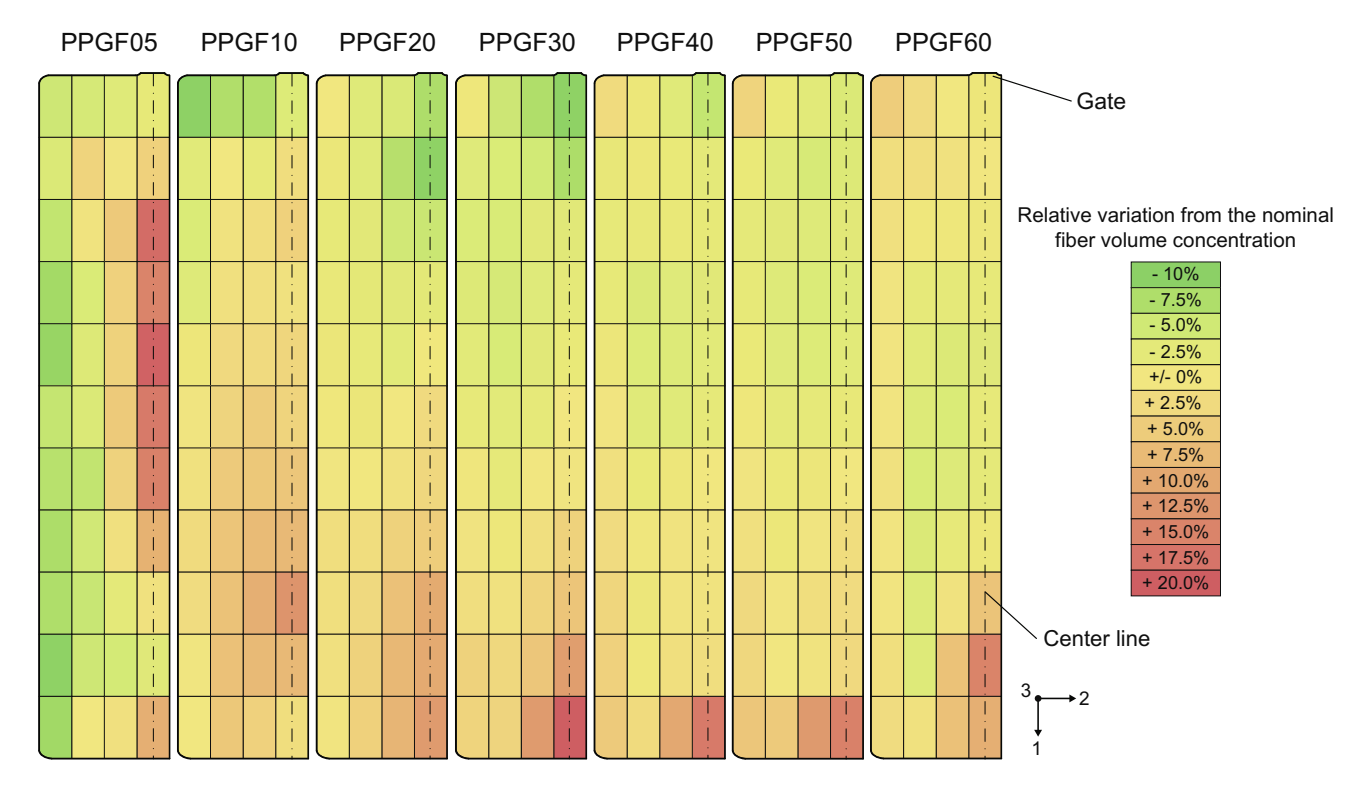


Fig. 8. Results of the global concentration gradient analysis for all trials. (For interpretation of the references to color in this figure legend, the reader is referred to the web version of this article.)

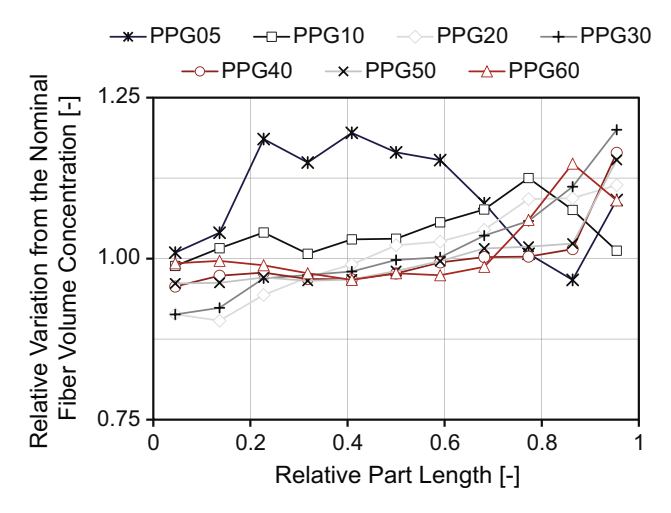


Fig. 9. Variation of fiber concentration along the plate length for all trials. (For interpretation of the references to color in this figure legend, the reader is referred to the web version of this article.)

Table 5Measured fiber concentration in the pellets and in the purged material.

Feed material	Nominal concentration [wt.%]	Measured concentration in the pellets [wt.%]	Measured concentration in the purged material [wt.%]
PPGF20 PPGF30 PPGF40 PPGF60	20 wt.% 30 wt.% 40 wt.% 60 wt.%	$\begin{array}{c} 19.82 \pm 0.44 \\ 29.32 \pm 0.49 \\ 39.56 \pm 0.63 \\ 59.49 \pm 0.29 \end{array}$	$\begin{array}{c} 19.99 \pm 0.08 \\ 29.45 \pm 0.27 \\ 39.72 \pm 0.10 \\ 59.30 \pm 0.23 \end{array}$

PPGF05 has a peak of up to 20% higher fiber concentration in the center of the plate. PPGF10 to PPGF60 show a tendency of depleted fiber concentration close to the gate and increased fiber concentration at the end of the flow.

Fig. 9 shows the variation of fiber concentration along the center-line of the molded part. The results for PPGF05 show a peak in the center of the plate for a large region (relative length 0.2-0.7). The other trials show a common trend of -5.2% less fibers close to the gate compared to the nominal fiber concentration and 11% more fibers at the end of the flow.

To evaluate the fiber concentration variation in the raw pellets caused by the material production, ten pellets were selected randomly and the weight fraction was determined through pyrolysis. The measurements were repeated ten times for the different pellet types used in this study. Additionally, the fiber concentration in the purged material was measured to investigate homogeneity of the material before the injection stage. The purged material was obtained by air shots at a retracted injection unit and the material was purged at 10% of the injection speed. Material from five air shots were recovered and measured. While the measured concentration in the pellets and the purged material are slightly below the nominal value, the measurements show that the fiber concentration is homogenous in the raw pellet material as well as after the plasticating phase in the purged material (Table 5).

4.2. Through-thickness concentration analysis using μ CT

Fig. 10 shows the measured through-thickness fiber concentrations at locations 1, 2 and 3 for all trials. The results suggest that the fiber concentration varies substantially in the thickness direction of all molded plates. The trials at higher concentrations (PPGF20 to PPGF60) show a common pattern in the measured con-

centration distribution. The measurements indicate a core layer with significantly higher fiber concentrations, which reach values of up to 1.5 times of the nominal concentration for PPGF40 (location 2). The shell layer and surface region have fewer fibers. For samples close to the gate (location 1), the width of the core layer is wider than at locations 2 and 3. There are also secondary concentration peaks close to the sample surfaces (relative thickness of ± 0.1), which reach values of 1.05 (PPGF20, location 2) to 1.45 (PPGF50, location 3). PPGF60 shows a fairly constant throughthickness concentration at the end of the flow path (location 3).

The trials at diluted suspensions (PPGF05 and PPGF10) show a different trend in through-thickness fiber concentration. At location 1, the core layers for both trials show a concentration minimum of 0.75 and maximum of 1.25 in the transition region between shell and core (relative thickness of approximately ± 0.3). PPGF05 shows a similar pattern of a minimum in the core enclosed by two maxima at locations 2 and 3 as well. On the other side, the PPGF10 results suggest a minor peak of approximately 1.1 in the core layer, which indicates a similar through-thickness pattern as found at higher concentrations.

For a more concise evaluation, two characteristic values can be defined: the core layer width δ and the maximum fiber concentration in the core layer ϕ_f^{max} , as illustrated in Fig. 11. The core layer width and maximum concentration measured at location 3 for all trials is shown in Fig. 12. The relative core width increases at higher nominal fiber concentrations from 0.10 at PPGF05 to 0.26 at PPGF60. While the maximum fiber concentration is 0.97 at PPGF05, it increases to 1.50 at PPGF40, which is the overall highest fiber concentration in the core found for all trials. For PPGF50 and PPGF60 it decreases to 1.36 and 1.27, respectively. The measurements for PPGF60 at location 3 a constant through-thickness fiber concentration and no distinct core layer.

4.3. Fiber packing density analysis

Fig. 13 summarizes the obtained average distance between fibers in the core and shell layer for all samples. As expected, the fiber spacing decreases from $68.1\,\mu\text{m}$ (PPGF05) to $11.6\,\mu\text{m}$ (PPGF60) with an increase in nominal fiber concentration. The findings at higher nominal fiber concentrations (PPGF20 to PPGF60) suggest that the average distance between fibers in the shell layer is larger than in the core layer. The difference between core and shell is the largest for PPGF20, PPGF30 and PPGF40, while it is lowest for PPGF60. The PPGF05 measurements show a slightly larger average distance between the fibers in the shell than in the core. For the PPGF10, the measured distance is almost the same for core and shell. Due to the scan resolution of 5.25 μm , the results for higher fiber concentrations (PPGF50 and PPGF60) should be treated cautiously in terms of the absolute distance values obtained in this study.

4.4. Flow front analysis

Partial mold fillings allow data to be obtained on the transient fiber configuration during the mold filling. Molding trials at 25%, 50%, 75% and 90% fill were done, and the fiber concentration was measured using μCT and pyrolysis. Fig. 14 shows a 3D reconstruction for the 50% fill.

Fig. 15 shows the measured through-thickness fiber concentration for the partially filled moldings at a nominal fiber concentration of 40 wt.% (PPGF40). The results suggest a fairly uniform fiber concentration through the thickness at the flow front without a distinct fiber agglomeration in the core layer for all fillings (Fig. 15 left), but a decreased fiber concentration towards the surface. At 10 mm from the flow front (Fig. 15 center), the measure-

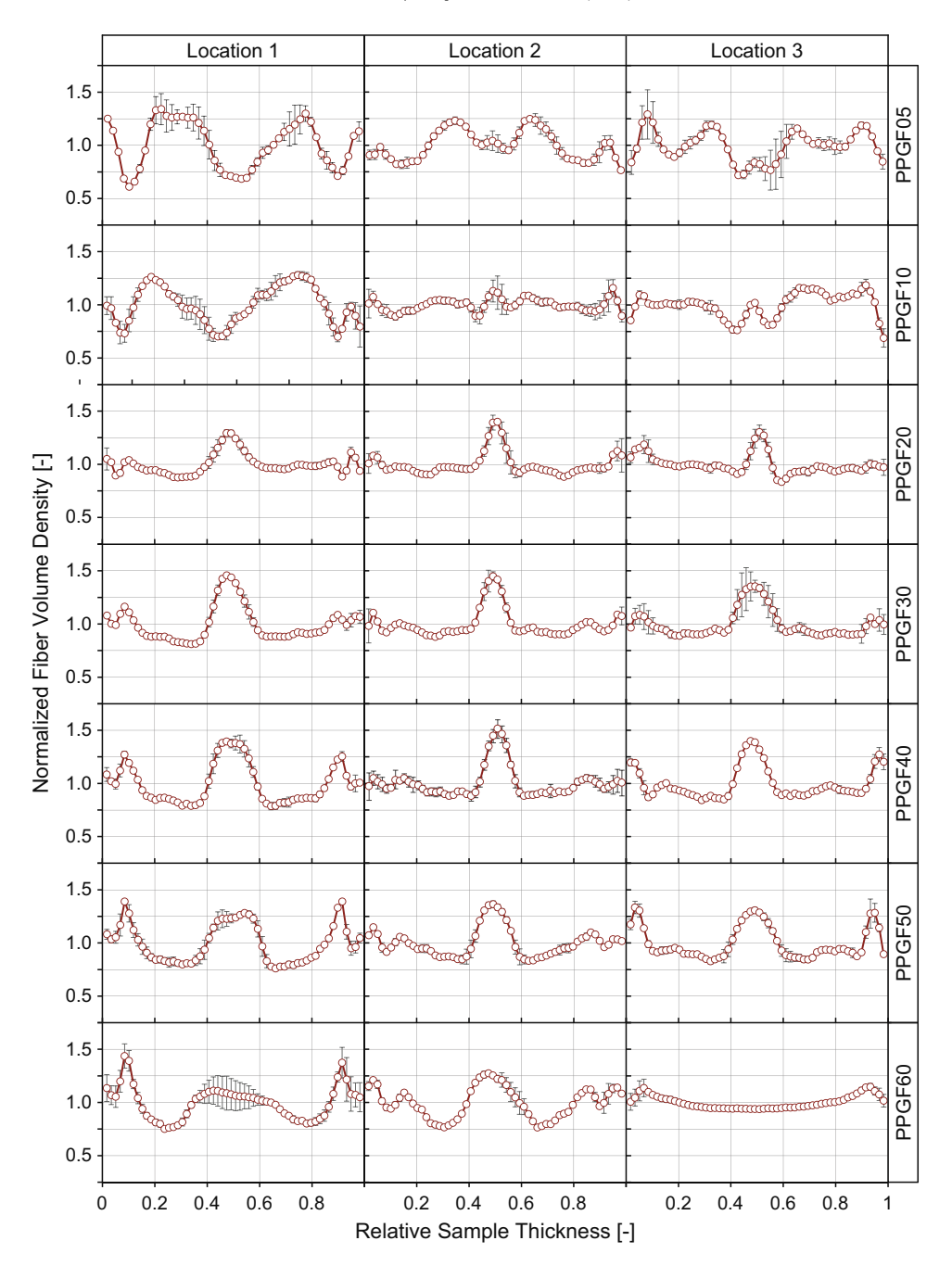


Fig. 10. Summary of the through-thickness fiber concentration of locations 1, 2 and 3 for all trials. (For interpretation of the references to color in this figure legend, the reader is referred to the web version of this article.)

ments suggest a fiber agglomeration in the core. The peak in fiber concentration in the core decreases with increasing mold fill with a nominal fiber concentration of 1.5 at 25% fill and 1.1 for 90%. The analysis of samples extracted 17 mm from the flow front show a more distinct core-shell structure. The peak of fiber concentration in the core shows a maximum of approximately 1.4 for 50%, 75% and 90% fill. For the 25% fill, the peak is larger at 1.6.

Additional measurements of the local fiber concentration through pyrolysis were performed to obtain the fiber concentration gradient along the flow length. Slices between 5 mm and 15 mm were cut from the partial mold fillings. Fig. 16 summarizes the measured fiber concentrations relative to the melt front (three repeated measurements per location). The measurements suggest a substantial peak at the flow front itself can be observed, which reaches between 48 wt.% for the 75% mold fill and up to 54.7 wt.

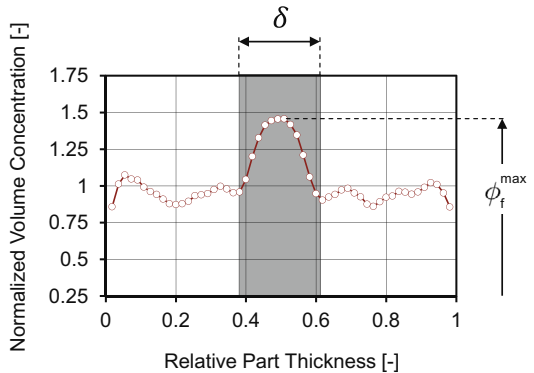


Fig. 11. Illustration of core layer thickness δ and fiber concentration maximum ϕ_j^{max} . (For interpretation of the references to color in this figure legend, the reader is referred to the web version of this article.)

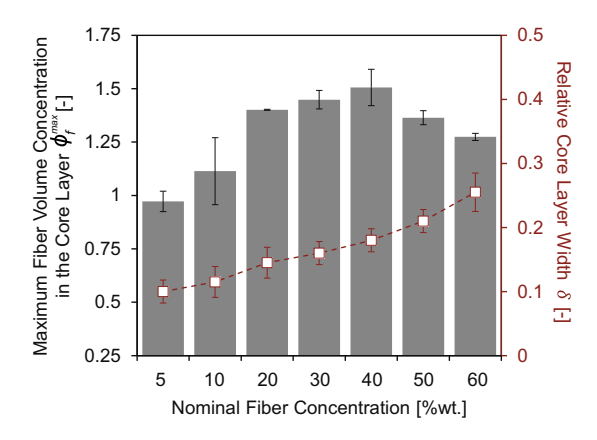


Fig. 12. Maximum fiber concentration in the core layer and core layer width at location 3 for all trials. (For interpretation of the references to color in this figure legend, the reader is referred to the web version of this article.)

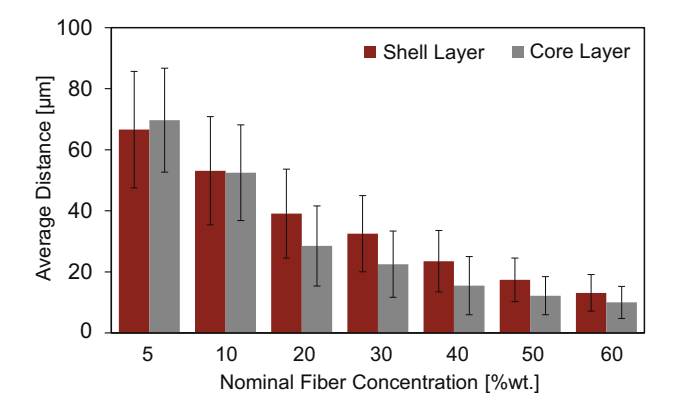


Fig. 13. Results of the fiber packing density analysis: Average distance between fibers in the shell and core layer. (For interpretation of the references to color in this figure legend, the reader is referred to the web version of this article.)

% for the 25% mold fill trial. Values above the nominal concentration (40 wt.%) are measured up to 25 mm from the flow front. At distances above 25 mm, the measured fiber concentration is on average 38.5 wt.%

5. Discussion

The results of this study show a non-uniform fiber concentration in the molded part. Fig. 17 shows a stitched set of low resolution μ CT scans of a complete PPGF40 plate (left) and 2D slices of

high resolution scans of the core layer and the shell layer respectively (right). This figure qualitatively highlights the fiber concentration gradients found in LFT injection induced by the process.

The heterogeneity can be divided into a global fiber concentration gradient throughout the entire molded plate and a throughthickness fiber concentration. The global concentration gradient for all trials shows increasing fiber concentration along the flow path. For all measurements except for PPGF05, the fiber concentration peaks at the end of the flow, while the samples close to the gate show a minimum. The findings are aligned with the outcome reported in other studies [6–11]. Although no clear explanation for this phenomenon has been established yet, a reasonable hypothesis for the variation is the interaction between partially embedded fibers and the molten core at the interface of the solidified layer during mold filling. Two mechanisms can take place, as shown in Fig. 18. Partially embedded fibers in the solidified layers are exposed to deformation and stresses caused by the advancement of the molten core during cavity filling. Ultimately, the fibers can be either sheared off or are pulled out and swept along with the molten core. Either mechanism can result in an increased fiber concentration at the last filled part of the cavity. The analysis of the fiber concentration of the partial mold fillings supports the theory because it shows a significant peak in fiber concentration at the melt front for all partial mold fillings, which suggests that an elevated concentration of fibers is carried along the flow front. Nevertheless, this hypothesis needs to be further tested by fiber length measurements along the flow path or at the melt front for partial mold filling. Longer fibers at the flow front would indicate that fiber pill-out might be the dominant mechanism.

The analysis of the through-thickness fiber concentration showed a substantial fiber agglomeration in the core layer and fewer fibers in the shell layers. Hence, the concentration distribution shows a core-shell pattern, which is commonly observed in fiber orientation measurements [28,29]. In terms of fiber orientation, this core-shell pattern is attributed to the fountain flow effect [4,30]. The fiber concentration distribution observed in this work might also be related to the fountain flow phenomenon, as the overall deformation at the flow front causes substantial reorientation of the fibers as they pass through the fountain flow. The material at the flow front is forced to move from the center of the cavity outwards onto the mold surfaces. The material freezes upon contact with the cold mold resulting in the formation of a solidified layer. As additional material enters the cavity, the advancing flow front is continuously stretched and rolls onto the cool wall where it freezes instantly. The high-shear region at the solidified layer and the advancing molten core causes a strong in-flow fiber alignment while the fibers in the core are oriented in cross-flow direction [31,32]. The degree of fiber alignment determines how closely the fibers can pack together, so the maximum fiber concentration

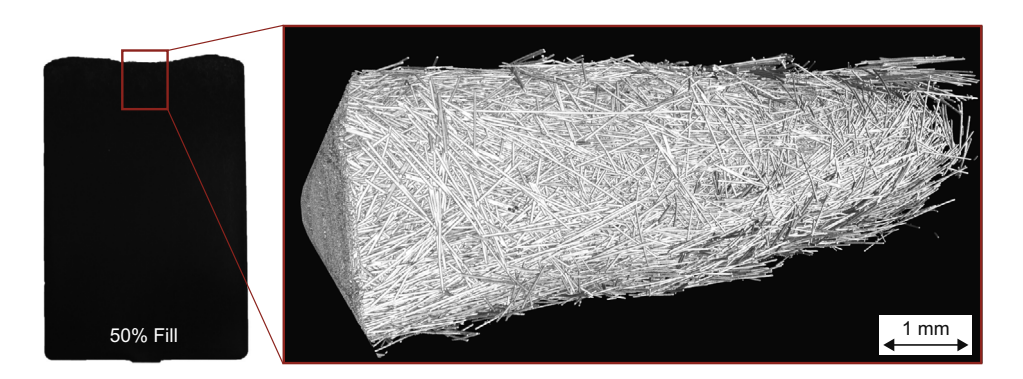


Fig. 14. Illustration of the flow front analysis: 3D reconstruction of the μCT scan of the flow front of the 50% mold fill at a nominal fiber concentration of 40 wt.% (PPGF40). (For interpretation of the references to color in this figure legend, the reader is referred to the web version of this article.)

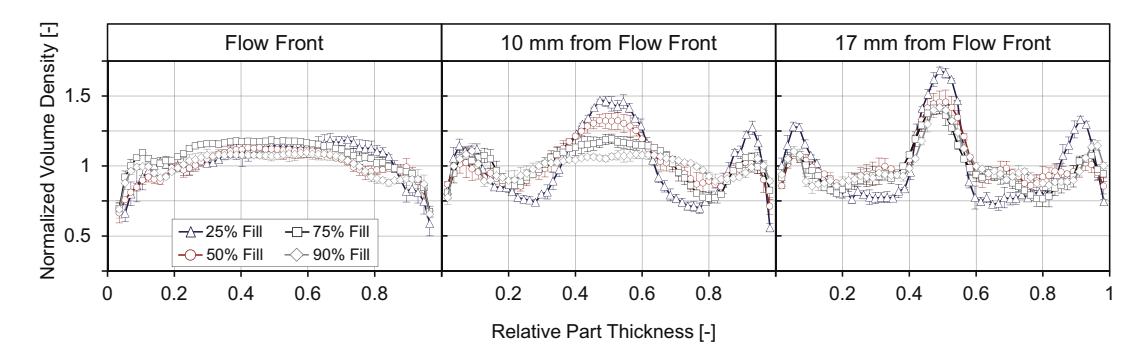


Fig. 15. Measured through-thickness fiber concentration of at the flow front for partially filled cavity molding (25%, 50%, 75% and 90% fill) at a nominal fiber concentration of 40 wt.% (PPGF40): At the flow front (left), 10 mm from the flow front (center) and 17 mm from the flow front (right). (For interpretation of the references to color in this figure legend, the reader is referred to the web version of this article.)

is directly related to the fiber orientation for concentrated suspensions.

The maximum three dimensional packing density for randomly aligned rods is determined by the volume fraction and the aspect ratio of the rod [33,34]. According to Milevski et al. [34], the product of volume fraction and aspect ratio equals 5.4 for randomly

aligned rods. The average fiber aspect ratio measured in the purged material for the PPGF40 trial is 80 ± 5.4 and the corresponding packing density is 6.57 vol.%, which is below the nominal fiber concentration of 19.1 vol.% At no point in the process is the fiber concentration low enough to allow a completely random fiber orientation, which implies that the fiber orientation will always

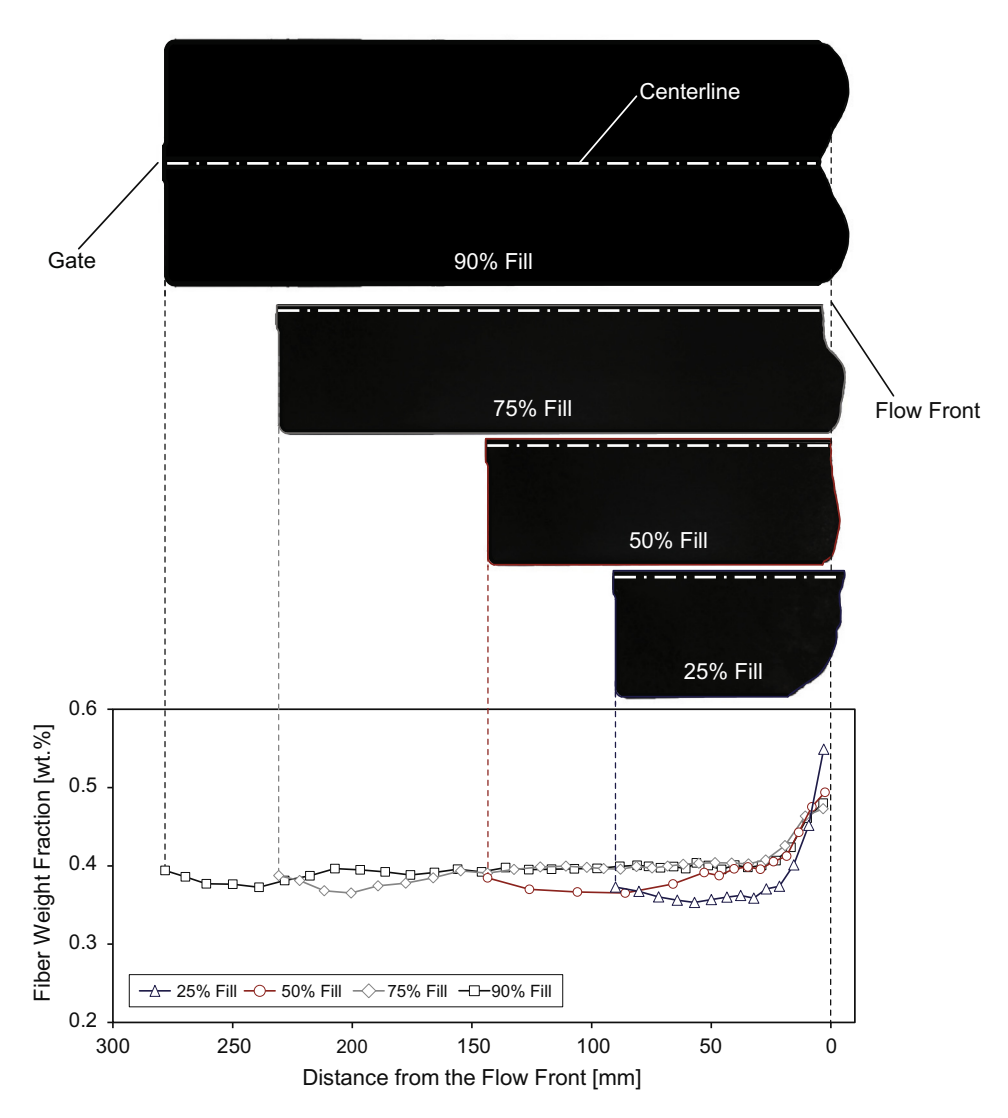


Fig. 16. Measured fiber concentration as a function of the distance to the flow front for partial mold fillings (25%, 50%, 75% and 90% fill) at a nominal fiber concentration of 40 wt.% (PPGF40). (For interpretation of the references to color in this figure legend, the reader is referred to the web version of this article.)

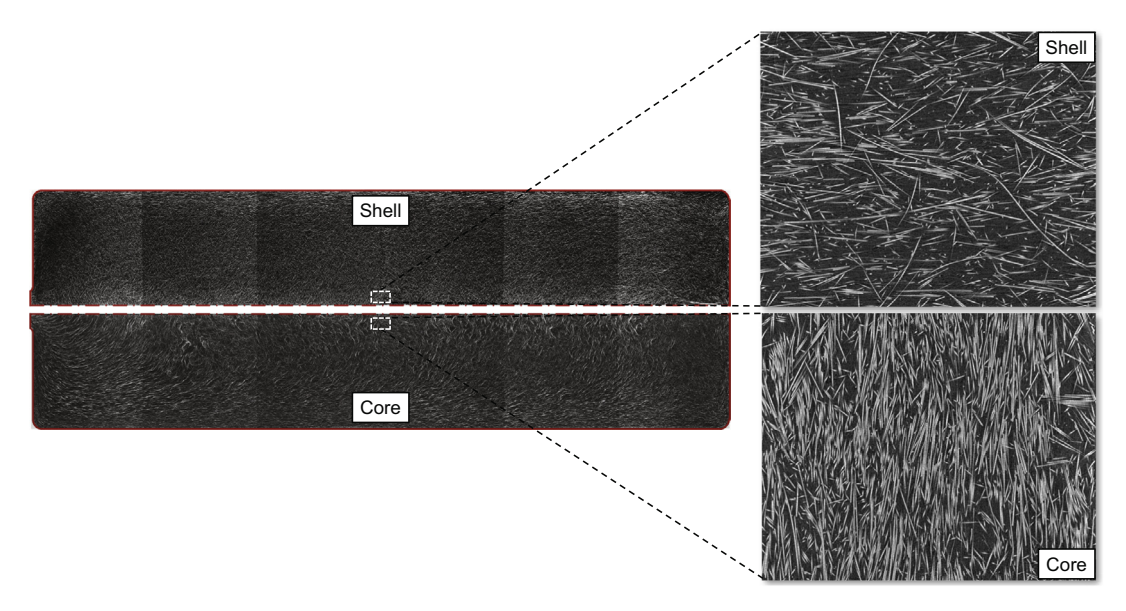


Fig. 17. Qualitative illustration of the process-induced fiber matrix separation in LFT injection molding for PPGF40: Stitched set of low resolution μ CT scans (left) and 2D slices of high resolution scans of the core layer and the shell layer (right). (For interpretation of the references to color in this figure legend, the reader is referred to the web version of this article.)

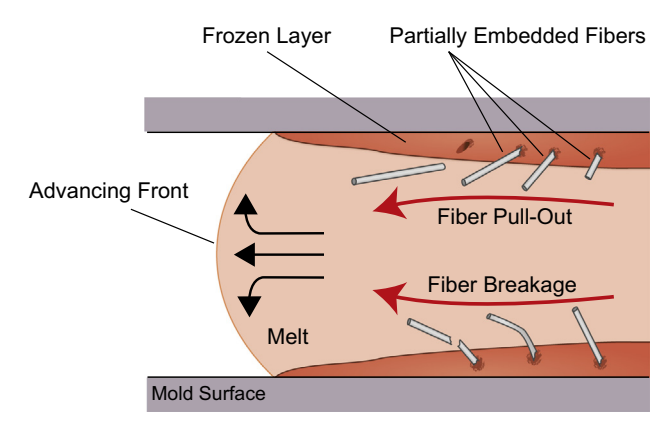


Fig. 18. Fiber pull-out and fiber breakage during cavity filling due to partly embedded fibers. (For interpretation of the references to color in this figure legend, the reader is referred to the web version of this article.)

be aligned to some degree. In particular, the fiber agglomeration found in the core requires a strong degree of fiber alignment to be able to pack together to at the concentration found in this study. This high packing density might not carry through the reorientation process at the advancing flow front. Hence, no substantial fiber concentration can be seen in the shell layers. Furthermore, Andersson and Toll [6] suggest that the fibers in the core are compressed by the fibers that move through the fountain flow. Furthermore, they argue that stresses emerge acting on the core layer fibers due to the elasticity of the fibers going through the reorientation process, which further compresses the fibers in the core layer and packs them more densely. This hypothesis would also explain why the trials at diluted concentrations (PPGF05 and PPGF10) show different trends in the through-thickness concentration. The low fiber concentration in these trials allows for more random fiber orientation throughout the part, and the alignmentconcentration dependence is not as pronounced.

6. Conclusion and outlook

This work summarizes a comprehensive experimental study on the fiber matrix separation in LFT injection molding. The results show that there are substantial concentration gradients within the molded part. Measurements of the raw pellet material and plasticated material before the injection phase (purged material) show a uniform fiber concentration. Hence, the observed nonuniform fiber concentration in the molded plates was identified to be caused by process-induced fiber matrix separation during cavity fill.

A measurement protocol using μ CT and image processing was developed and validated with conventional subtractive machining. The results show that the μ CT analysis offers several advantages, including fine resolution and time efficient analyses, as well as being non-destructive and allowing additional measurements such as fiber orientation measurements or void detection. For all trials, the through-thickness fiber concentration shows substantial accumulations of fibers in the core layer, refuting the common assumption of a uniform fiber concentration in injection molded LFT parts. For PPGF40, the measurements suggest 1.5 times the nominal fiber concentration in the core layer. The degree of fiber matrix separation observed in this study has significant implications for the prediction of the process-induced microstructure as well as modeling the material response in structural analyses.

An important avenue to explore is how the rheological behavior of the suspension influences fiber migration. Tozzi et al. [35] showed experimentally that the velocity profile of cellulose fiber-filled suspensions strongly depends on the local fiber concentration. However, the fiber orientation [36] and fiber length [37] affect the suspension rheology as well. An important next step would be a fundamental experimental study on the effect of the rheological properties on fiber matrix separation while accounting for any changes in fiber length and fiber orientation. Furthermore, the effect of the gate design and flow type on the process-induced fiber matrix separation should also be investigated. The type of gate might change the migration in the gate region and could provide further insight in the underlying mechanism of fiber migration.

First attempts to predict the fiber matrix separation during injection molding have been made [18,19] based on the suspension balance model assuming shear-induced particle migration. This approach completely neglects the reorientation mechanism as well as the relationship between fiber alignment and fiber concentration. On the other hand, fiber orientation models based on the

Folgar-Tucker model describe the orientation process as a rotary diffusion mechanism related to fiber-fiber interactions [4]. However, the rotary diffusion models assume a constant fiber concentration throughout the entire process. Hence, the process-induced change in concentration during molding is not taken into account for the fiber orientation prediction. Based on the findings of this work, a coupled approach between orientation and concentration would be recommended for predicting the final fiber microstructure.

The vast majority of structural analyses assume a uniform fiber concentration throughout the part, but the observed process-induced variation in fiber concentration may have a substantial impact on the material response. In particular, the through-thickness fiber concentration with a fiber agglomeration in the core layer would need to incorporated. It can be expected that the core layer and the fiber alignment in that layer contributes significantly more to the mechanical performance compared to the common assumption of a constant fiber concentration. Furthermore, the fiber accumulation found at the flow front observed is expected to influence the fiber configuration at weld lines and the further exploration would be of interest.

Acknowledgements

The authors wish to thank the National Science Foundation for financially supporting this work (Award #1633967). The authors also thank SABIC Global Technologies B.V. for their financial support, technical input and for providing the material used in this work. Mr. Goris would like to acknowledge the financial support provided by the Dr. Jackie Rehkopf Scholarship, awarded to him by the *Society of Plastics Processing* (SPE) Composites and Automotive Divisions.

References

- [1] Osswald TA, Menges G. Materials science of polymers for engineers. 3rd ed Munich: Hanser Publisher: 2012
- [2] Goris S, John P, Osswald TA. Chapter 33: polymer composites manufacturing processes. In: Manufacturing engineering handbook. McGraw-Hill Education; 2015
- [3] Phelps JH, Abd El-Rahman AI, Kunc V, Tucker CL. A model for fiber length attrition in injection-molded long-fiber composites. Compos Part A: Appl Sci Manuf 2013;51(0):11–21.
- [4] Folgar F, Tucker CL. Orientation behavior of fibers in concentrated suspensions. J Reinf Plast Compos 1984;3(2):98–119.
- [5] Londoo-Hurtado A, Hernandez-Ortiz JP, Osswald TA. Mechanism of fiber matrix separation in ribbed compression molded parts. Polym Compos 2007;28(4):451–7.
- [6] Toll S, Andersson P-O. Microstructure of long- and short-fiber reinforced injection molded polyamide. Polym Compos 1993;14(2):116–25.
- [7] O'Regan D, Akay M. The distribution of fibre lengths in injection moulded polyamide composite components. J Mater Process Technol 1996;56 (14):282–91. International conference on advances in material and processing technologies.
- [8] Lafranche E, Krawczak P, Ciolczyk J-P, Maugey J. Injection moulding of long glass fiber reinforced polyamide 66: processing conditions/microstructure/ flexural properties relationship. Adv Polym Technol 2005;24(2):114–31.
- [9] Kubat J, Syalanczi A. Polymer-glass separation in the spiral mold test. Polym Sci Eng 1974;14(12).
- [10] Hegler RP, Mennig G. Phase separation effects in processing of glass-bead- and glass-fiber-filled thermoplastics by injection molding. Polym Eng Sci 1985;25 (7):395–405.

- [11] Ogadhoh SO, Papathanasiou TD. Particle rearrangement during processing of glass-reinforced polystyrene by injection moulding. Compos Part A: Appl Sci Manuf 1996;27(1):57–63.
- [12] Mondy LA, Brenner H, Altobelli SA, Abbott JR, Graham AL. Shear induced particle migration in suspensions of rods. J Rheol 1994;38(2):444–52.
- [13] Vlez-Garca GM, Wapperom P, Baird DG, Aning AO, Kunc V. Unambiguous orientation in short fiber composites over small sampling area in a centergated disk. Compos Part A: Appl Sci Manuf 2012;43(1):104–13.
- [14] Sun X, Lasecki J, Zeng D, Gan Y, Su X, Tao J. Measurement and quantitative analysis of fiber orientation distribution in long fiber reinforced part by injection molding. Polym Test 2015;42(0):168–74.
- [15] Leighton David, Acrivos Andreas. The shear-induced migration of particles in concentrated suspensions. J Fluid Mech 1987;181:415–39.
- [16] Nott Prabhu R, Brady John F. Pressure-driven flow of suspensions: simulation and theory. J Fluid Mech 1994;275:157–99.
- [17] Morris Jeffrey F, Boulay Fabienne. Curvilinear flows of noncolloidal suspensions: the role of normal stresses. J Rheol 1999;43(5):1213–37.
- [18] Tseng Huan-Chang, Chang Yuan-Jung, Hsu Chia-Hsiang. Prediction of fiber microstructure for injection molding: orientation, degradation, and concentration. In: Proceedings of the SPE automotive composites conference & exhibition (ACCE); 2014.
- [19] Tseng H-C, Wang T-C. Progress on fiber concentration for injection molding simulation of fiber reinforced thermoplastics. In: Proceedings of the ANTEC, Orlando: 2014.
- [20] Kuhn Christoph, Walter Ian, Taeger Olaf, Osswald Tim. Experimental and numerical analysis of fiber matrix separation during compression molding of long fiber reinforced thermoplastics. J Compos Sci 2017;1(2).
- [21] SABIC. SABIC STAMAX material datasheet; 2017.
- [22] SABIC. Processing guides: SABIC Stamax; 2016.
- [23] Stock SR. MicroComputed tomography: methodology and applications. Boca Raton: CRC Press; 2009.
- [24] Buck F, Brylka B, Mller V, Mller T, Weidenmann KA, Hrymak AN, et al. Two-scale structural mechanical modeling of long fiber reinforced thermoplastics. Compos Sci Technol 2015;117:159–67.
- [25] Perez C, Goris S, Osswald TA. Study on the fiber properties of a LFT strand. In: SPE automotive composites conference & exhibition (ACCE), 13th annual; 2013.
- [26] Carmignato Simone, Dewulf Wim, Leach Richard, editors. Industrial X-ray computed tomography. Cham: Springer International Publishing; 2018. https://doi.org/10.1007/978-3-319-59573-3 1.
- [27] Schindelin Johannes, Arganda-Carreras Ignacio, Frise Erwin, Kaynig Verena, Longair Mark, Pietzsch Tobias, et al. Fiji: an open-source platform for biological-image analysis. Nat Meth 2012;9(7):676–82.
- [28] Bay Randy S, Tucker Charles L. Fiber orientation in simple injection moldings. Part II: Experimental results. Polym Compos 1992;13(4):332–41.
- [29] Foss PH, Tseng H-C, Snawerdt J, Chang Y-J, Yang W-H, Hsu C-H. Prediction of fiber orientation distribution in injection molded parts using Moldex3d simulation. Polym Compos 2014;35(4):671–80.
- [30] Tadmor Z. Molecular orientation in injection molding. J Appl Polym Sci 1974;18(6):1753–72.
- [31] Phelps JH, Tucker CL. An anisotropic rotary diffusion model for fiber orientation in short- and long-fiber thermoplastics. J Non-Newton Fluid Mech 2009;156(3):165–76.
- [32] Tseng Huan-Chang, Chang Rong-Yeu, Hsu Chia-Hsiang. Improved fiber orientation predictions for injection molded fiber composites. Compos Part A: Appl Sci Manuf 2017:99:65-75.
- [33] Philipse Albert P. The random contact equation and its implications for (colloidal) rods in packings, suspensions, and anisotropic powders. Langmuir 1996:12(5):1127–33.
- [34] Milewski JV. The combined packing of rods and spheres in reinforcing plastics. Ind Eng Chem Prod Res Dev 1978;17(4):363–6.
- [35] Tozzi EJ, Lavenson DM, McCarthy MJ, Powell RL. Effect of fiber length, flow rate, and concentration on velocity profiles of cellulosic fiber suspensions. Acta Mech 2013;224(10):2301–10.
- [36] Laun HM. Orientation effects and rheology of short glass fiber-reinforced thermoplastics. Colloid Polym Sci 1984;262(4):257–69.
- [37] Huq AMA, Azaiez J. Effects of length distribution on the steady shear viscosity of semiconcentrated polymer-fiber suspensions. Polym Eng Sci 2005;45 (10):1357–68.